

Article

Mechanical, Dielectric, and Thermal Attributes of Polyimides Stemmed Out of 4, 4′-Diaminodiphenyl Ether

Panpan Zhang ^{1,*}, Ke Zhang ², Shuliang Dou ^{3,*}, Jiupeng Zhao ², Xiangqiao Yan ³ and Yao Li ^{3,*} ¹ Jincheng Campus, Taiyuan University of Science and Technology, Jincheng 048011, China² MIIT Key Laboratory of Critical Materials Technology for New Energy Conversion and Storage, School of Chemistry and Chemical Engineering, Harbin Institute of Technology, Harbin 150001, China; zhangke@hit.edu.cn (K.Z.); jpZhao@hit.edu.cn (J.Z.)³ Center for Composite Materials and Structures, Harbin Institute of Technology, Harbin 150001, China; yanxiangqiao406@163.com

* Correspondence: Zpanpan1989@163.com (P.Z.); DouSl@hit.edu.cn (S.D.); yaoli@hit.edu.cn (Y.L.)

Received: 21 January 2020; Accepted: 4 March 2020; Published: 5 March 2020



Abstract: Several kinds of polyimide (PI) films stemmed out of 4, 4′-diaminodiphenyl ether, as well as various structurally various aromatic dianhydride, were prepared. The films' mechanical, dielectric, and dynamic mechanical attributes were put under investigation. According to the findings, the PI films' performance is significantly different as a result of their diverse structure. PI's dielectric constant and dielectric loss tangent of abides by the increasing order below: PMDA-PI > BTDA-PI > BPDA-PI. Moreover, the electric breakdown strength of BTDA-PI (478.90 kV/mm) presents a lot higher value compared to the one PMDA-PI (326.80 kV/mm) and BPDA-PI (357.07 kV/mm). In particular, BTDA-PI film possesses high electric breakdown strength about 478.90 kV/mm. In addition, PI's glass transition temperature (T_g) are, respectively, 276 °C (BTDA-PI), and 290 °C (BPDA-PI), as well as 302 °C (PMDA-PI). Therefore, in virtue of their various structures and performances, practical applications of PI films can exert significant role in the electronics and microelectronics industries.

Keywords: polyimide; film; dielectric properties; thermal properties

1. Introduction

Aromatic polyimides (PIs) have been deemed as crucial high-performance polymers classes based on the integration of excellent mechanical, electrical, and thermal properties, as well as chemical and solvent resistance [1–5]. Therefore, these materials are being used in numerous applications, which range from engineering plastics under aerospace industries to the films for the printed electronic circuitry applications [6–9], as a result of the superior excellent dimensional stability, the temperature under high glass transition, good optical transparency, good electrical resistivity, low water absorption, and relative permittivity [10–13]. PIs are mainly used by taking the type of films and moldings, as well as foams [14]. PIs have been particularly applied in a broad range as high-performance films, such as microelectronics, gas or solvent separation, non-linear optical devices, aerospace engineering, and printed electronic circuitry.

DuPont's Kapton type film has been boasting one of the most representative and successful commercial PI film over the past decades. The typical Kapton PI was obtained from pyromellitic dianhydride (PMDA), along with 4,4′-diaminodiphenyl ether (ODA). Moreover, ever since the commercialization of the Kapton type PI began the usage in the early 1960s, a series of PIs composed of different diamine and dianhydride have been reported [15–18]. However, for the structurally different PIs, their properties are different, as well. Therefore, it is necessary to conduct explorations on

their structure–property relationships for practical applications. Although some studies showed that the chain hardness constituted the extremely crucial factor which affects their attributes in a direct way [19–23], the structure–property relationships links PIs are still not well understood.

In this regard, we prepared several different PIs obtained from ODA and multiple structured-based distinct aromatic dianhydrides and investigated their properties. The effect of structural changes in PI films' mechanical, dielectric, and thermal attributes was studied, which was oriented with a better understanding of PI films' structure–property relationships in practical applications.

2. Experiential

2.1. Materials

The achievement of pyromellitic dianhydride (PMDA), 3,3',4,4'-benzophenonetetracarboxylic dianhydride (BTDA), and 3,3',4,4'-biphenyltetracarboxylic dianhydride (BPDA), together with 4,4'-diaminodiphenyl ether (ODA), was conducted in Beijing Yinuokai Technology Co., Ltd. (Beijing, China). The purchase of N, N-dimethylacetamide, DMAC (99.0%) was made in Shanghai Aladdin Bio-Chem Technology Co., Ltd. (Shanghai, China). The overall reagents, which took on analytical reagent (AR) level, were employed to start materials with no more purification.

2.2. Integration of PI Films

The synthesis of PI films was conducted in virtue of standard two-phase-based procedure as follows. First, dissociation of ODA (10 mmol, 2.00 g) was implemented in a clean 50 mL, 3-neck- round bottom flask with DMAC solvent (20 mL) and then stirred for 15 min. The BTDA (10 mmol, 3.22 g) was added continuously for several times. Then, the mixed liquid was given 4-hour of vigorous stirring to produce a sticky and uniform polyamic acid solution. After that, the polyamic acid solution was coated on a glass plate, heated in a vacuum oven at 60 °C for 2 h, and then subjected to 1-hour thermal imidization at individual temperatures of 100 °C, 200 °C, and 300 °C in dry-air-flowing oven. In the last step, the BTDA-PI film was made by the experimental preparation above. The PMDA-PI and BPDA-PI were prepared in virtue of a similarly-structured process as above. The film was made with nearly 30–35 μm. Figure 1 presents the synthesis process of PI films.

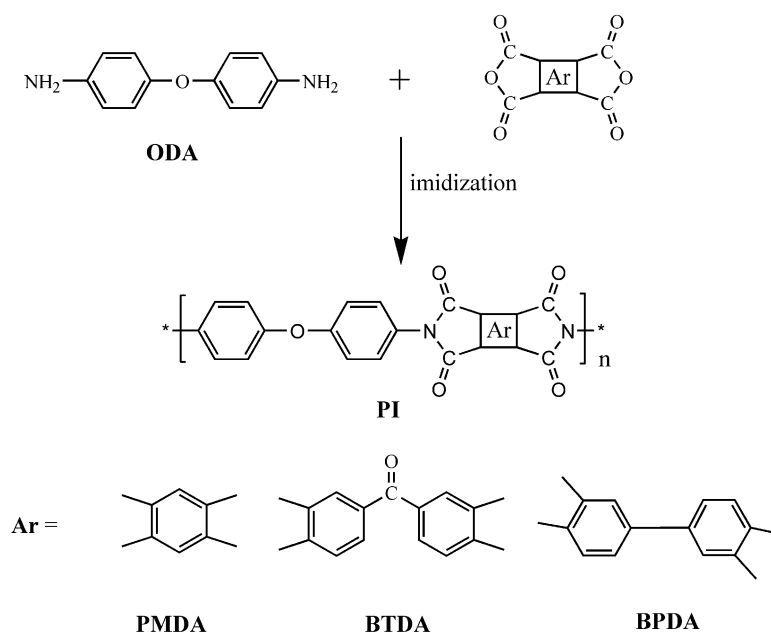


Figure 1. Synthesis process of polyimide (PI) films. ODA = 4,4'-diaminodiphenyl ether; PMDA = pyromellitic dianhydride; BTDA = 3,3',4,4'-benzophenonetetracarboxylic dianhydride.

2.3. Characterization and Tests

The structure of the film was put under the research of Fourier transform infrared (FTIR) spectroscopy (Nicolet Avatar-360, Thermo Nicolet Corporation, Waltham, MA, USA) and X-ray diffraction (XRD) spectroscopy (Rigaku Dmax-rB, Rigaku Corporation, Tokyo, Japan). XRD was conducted in virtue of Cu K α radiation ($\lambda = 1.5406 \text{ \AA}$). The test on films' insulating and dielectric attribute was carried out through the highly-intensified megohm micro electric current tester (ST2255, Suzhou Lattice Electronics Co., Ltd, Suzhou, China) and impedance analyzer (Agilent4294A, Agilent Technologies Corporation, Santa Clara, CA, USA), respectively. The electric breakdown performance got experimented in virtue of a dielectric withstand voltage test (YD2013, Changzhou Yangzi Electronic Co., Ltd, Changzhou, China). The mechanical tests of the films was carried out by a micro electronic testing machine (WDW-20, Jinan Fangyuan Testing Machine Co., Ltd, Jinan, China). The performance of dynamic mechanical analysis (DMA) was committed on a sample with the size of $30 \times 5 \times 0.5 \text{ mm}^3$ in virtue of a dynamic mechanical analyzer of TA Instruments (DMAQ 800, TA Instruments Corporation, New Castle, DE, USA), and the stretched film mode was carried out at a temperature ranging from ambient temperature to $200 \text{ }^\circ\text{C}$ (1 Hz) with the heating ratio of $5 \text{ }^\circ\text{C}$ per min.

3. Findings and Discussions

3.1. PI Films' Structure

PI films are structured by the chemical structures which were tested via FT-IR spectroscopy, as Figure 2a displays. Figure 2a offered the findings of the structure's peak, which is at 725 cm^{-1} , 1376 cm^{-1} , 1719 cm^{-1} and 1774 cm^{-1} . The results individually correspond to C=O bending, C-N stretching, and C=O symmetric stretching, as well as asymmetric stretching. An imide's structure can be confirmed.

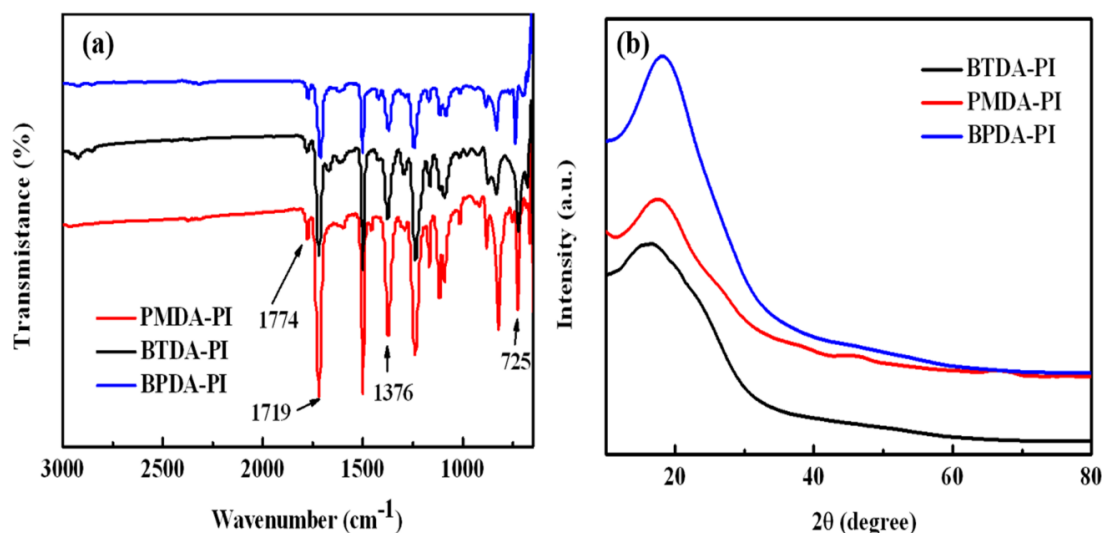


Figure 2. FT-IR spectra (a) and XRD patterns (b) of PI films.

Figure 2b shows the X-ray diffraction types of three kinds of PI films. Three broad peaks can be placed under apparent observation within the range of about $2\theta = 16\sim 19^\circ$, which confirms the ordered region in amorphous polyimide. These broad peaks are mainly originated from the partial crystallization of PI films. However, we also can notice that the strength and shape of the peaks is similar. Therefore, DMA analysis was further used to investigate the crystalline degree of PI in the following discussion.

3.2. Mechanical Properties of PI Films

The tensile strength, tensile modulus, and elongation at the break of PI films are summarized in Figure 3. It can be apparently observed that the BPDA-PI film has a better plastic property, and the elongation at the break of it is as high as 3.8%. PMDA-PI possesses a higher brittleness with the high tensile modulus of 3.42 GPa and low elongation at of 2.82%. It should be further addressed that the BTDA-PI shows an excellent comprehensive performance with the high tensile strength of 114.19 MPa, the tensile modulus of 3.23 GPa and elongation at the break of 3.58%. The diversity of tensile properties could be attributed to different molecular chain flexibility and intermolecular force in the PI films.

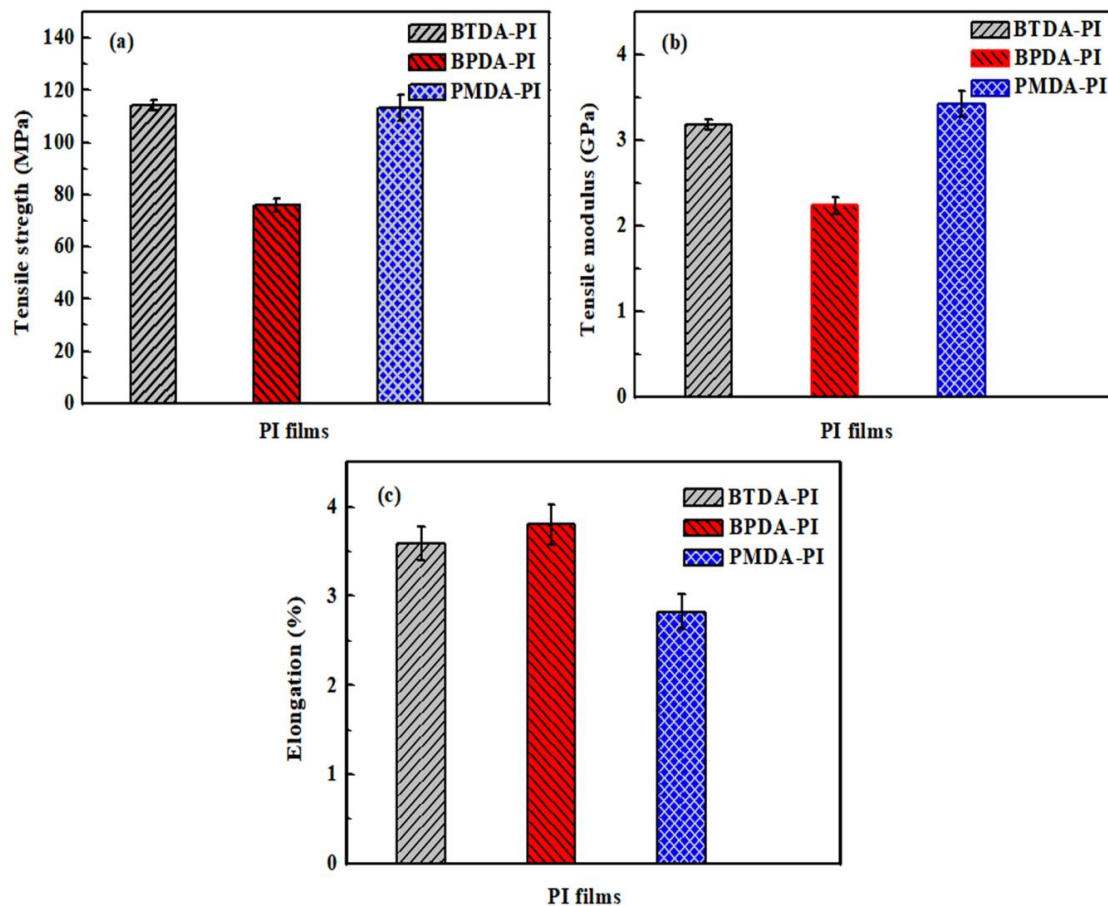


Figure 3. The mechanical properties of PI films: (a) tensile strength, (b) tensile modulus, and (c) percent elongation at break.

3.3. Dielectric Attributed Harbored by PI Films

Figure 4a shows the relative dielectric constant of PI films at the frequency of 50~10⁶ Hz on the condition of room temperature. The dielectric constants of PI films, which features relatively more stability from 50 to 10⁴ Hz, expressed a decreasing trend in the high-frequency from 10⁴ to 10⁶ Hz. Moreover, the dielectric constants presented significant distinction for three kinds of PI films. The constants of the PI film varied between 3.39~3.69 at 100 Hz. PI, based on the dielectric constant of ODA, were sticking to the following increasing order: PMDA-PI > BTDA-PI > BPDA-PI. This phenomenon can be attributed to the different molecular polarity caused by the different molecular chain structure. The Clausius-Mossotti equation can be used to explain the dielectric constant of PI membranes [24]:

$$\frac{\epsilon_r - 1}{\epsilon_r + 2} = \frac{N\alpha}{3\epsilon_0}, \quad (1)$$

where ϵ_r is the dielectric constant; ϵ_0 is the vacuum permittivity; N is the molecule number in unit volume; and α is the molecular polarization. According to Equation (1), the various dielectric constant of ODA based PI can be mainly attributed to the different molecular polarization caused by the different molecular chain structure.

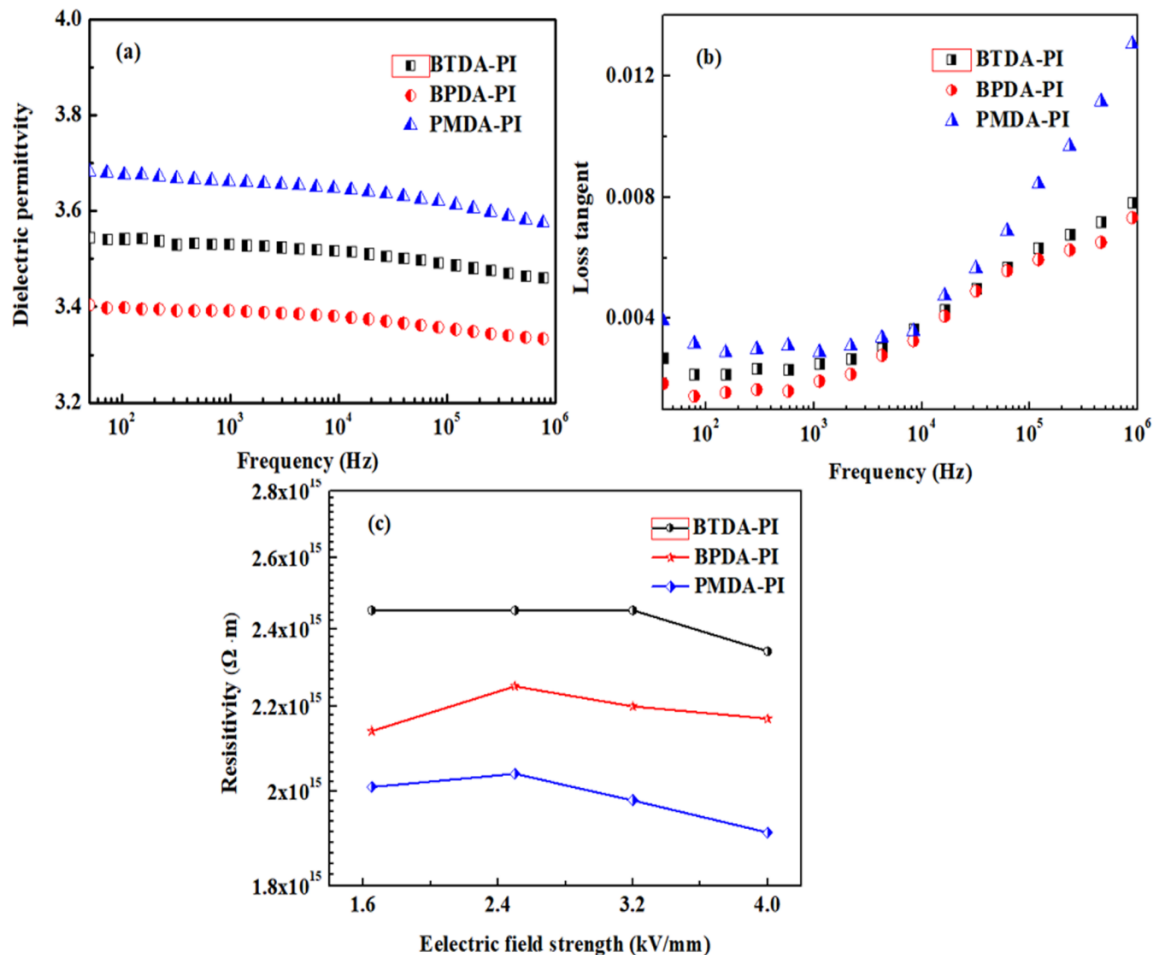


Figure 4. Variations of (a) dielectric permittivity, (b) loss tangent, and (c) resistivity of PI films.

The dielectric loss tangent of PI films is given in Figure 4b. According to the observation, as the frequency increases, the loss tangent first drops slightly and then rises sharply. The dielectric loss mainly arises out of relaxation polarization and inter-facial polarization here. Within the $50 \sim 10^3$ Hz frequency range, the dielectric loss tangent decreases slightly, which is caused by the interface polarization lagging behind the change of electric field frequency. The increase range from 10^4 to 10^6 Hz is attributed to PI's glass transition relaxation [25]. Moreover, it is observed that the dielectric loss tangent of PI was also abiding by the following increasing order: PMDA-PI > BTDA-PI > BPDA-PI. However, all PI show a lower dielectric loss tangent. Besides, even for PMDA-PI films, the loss tangent still features less value compared to 0.004 at 100 Hz.

To investigate the insulating property to the films, volume resistivities were tested at different electric field strengths, and representative results are expounded in Figure 4c. As can be seen in the figure, all of the three films show high resistivities (10^{15} Ωm) and confirm PI films' excellent insulativity. Moreover, the three films harbor the resistivity values, which present a slight difference, which might be attributable to the various strength of the conjugate effect in the PI molecules.

3.4. Breakdown Strength Harbored by PI Films

The measurement of PI films' dielectric breakdown was taken on the condition of room temperature. Dielectric breakdown is discussed in virtue of a two parameters Weibull distributions as follows [24]:

$$P(E) = 1 - e^{-(E/\alpha)^\beta}, \quad (2)$$

where $P(E)$ refers to the cumulative probability of the failure which occurred in at the electric area with a low or equal value to E . E means the experimental breakdown strength; α stands for the proportional parameter, which presents the breakdown strength when 63.2% is expressed as the cumulative failure probability. β is a shape parameter which is relevant to a linear regression fit in the distribution. The Weibull cumulative distribution function could be described as the following two logarithms:

$$\ln(-\ln(1 - P(E))) = \beta \ln E - \beta \ln \alpha. \quad (3)$$

Next, $\ln(-\ln(1 - P(E)))$ versus $\ln E$, was sketched. The values could be, respectively, achieved out of the slope, the $\ln(-\ln(1 - P(E)))$ interception and $\beta \ln \alpha$. α and β are decided by least-squares linear regression. Table 1 includes the linear fitting results and PI films' Weibull parameters. According to Table 1, the correlation coefficient (R) values presented higher value compared to 0.95. That reveals a fine fitting upon the PI films. Figure 5 shows the PI films' Weibull deploy. As is seen, the PMDA-PI harbors the breakdown strength which is close to BPDA-PI. Nonetheless, the breakdown strength harbored by BTDA-PI (478.90 kV/mm) presents far higher value compared the one of PMDA-PI (326.80 kV/mm) and BPDA-PI (357.07 kV/mm). It might be due to the different crystalline degree and regularity in the PI molecular structure films.

Table 1. Linear fitting results and Weibull parameters of PI films.

PI Films	Linear Fitting Results			Weibull Parameters	
	Slope	$\ln(-\ln(1 - P(E)))$ Intercept	R	β	α/kVmm^{-1}
BTDA-PI	9.68	-59.74	0.9702	9.68	478.90
BPDA-PI	10.65	-62.60	0.9612	10.65	357.07
PMDA-PI	4.13	-23.91	0.9547	4.13	326.80

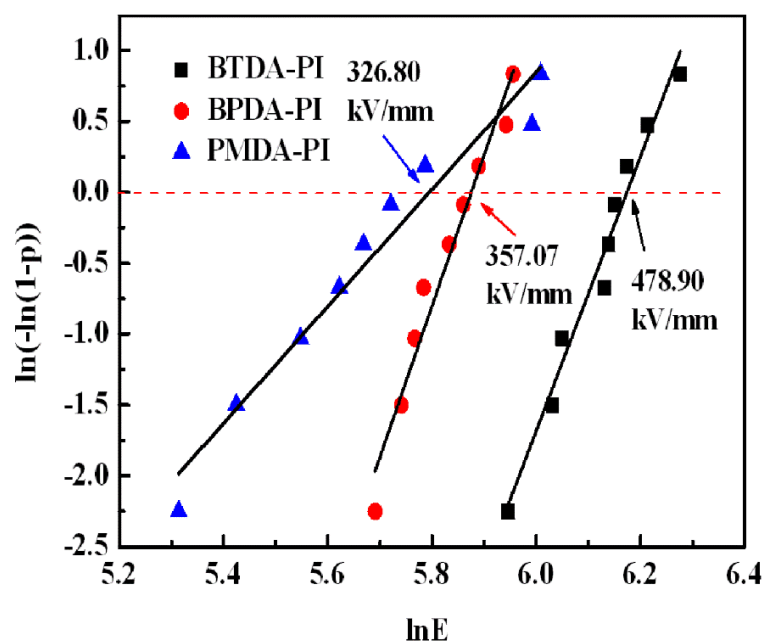


Figure 5. Weibull distribution of PI films.

3.5. Thermal Properties Harbored by PI Films

Thermal stability contributes as a major performance for PI engineering films. Figure 6 interprets differential DMA curves announce the different glass transition temperature (T_g) of PI. Therefore, it is clear that the glass transition temperature of PI films are 276 °C (BTDA-PI), 290 °C (BPDA-PI), and 302 °C (PMDA-PI), respectively. The DMA results confirm that the expression of the thermal stability harbored by PI in the below increasing order: PMDA-PI>BTDA-PI>BPDA-PI. Moreover, the DMA results indirectly show the crystalline degree of the PI films maybe in the following increasing order: PMDA-PI>BTDA-PI>BPDA-PI. Thereby, it is of significance in the practical application of PI films according to their different thermal properties.

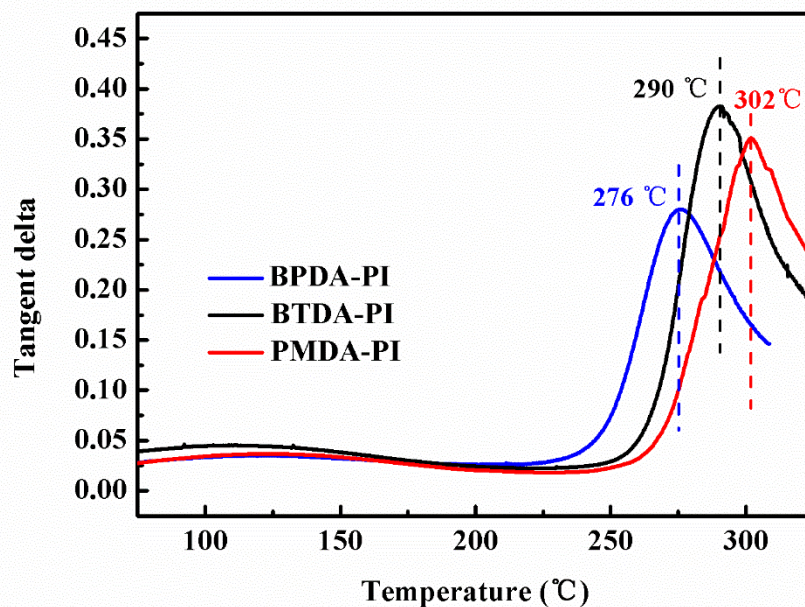


Figure 6. DMA curves of the PI films.

4. Conclusions

In summary, the preparations of several varied aromatic PIs got out of the standard two-phase procedure of diamine (ODA) with various structurally different dianhydrides (PMDA, BTDA, and BPDA). The dielectric and thermal properties were measured for the research on the three kinds of PI films. It is found that BTDA-PI film possesses an excellent comprehensive tensile properties. The dielectric properties of the three films is marking a slight difference since the different molecular polarity and conjugate effect of PI molecules. The PI, which is based on the dielectric constant and dielectric loss tangent of ODA-based are existing in the following increasing order: PMDA-PI>BTDA-PI>BPDA-PI. In particular, BTDA-PI film possesses high electric breakdown strength about 478.90 kV/mm. In addition, the glass transition temperature of PI films are 276 °C (BTDA-PI), 290 °C (BPDA-PI), and 302 °C (PMDA-PI), respectively. Therefore, in terms of their various structures and performances, it is a significant job to conduct practical applications of PI films in the electronics and microelectronics industries.

Author Contributions: Conceptualization, P.Z. and Y.L.; methodology, K.Z., J.Z. and P.Z.; software, P.Z. and X.Y.; validation, P.Z., K.Z. and S.D.; formal analysis, P.Z.; investigation, P.Z.; resources, Y.L. and J.Z.; data curation, P.Z.; writing—original draft preparation, P.Z. and K.Z.; writing—review and editing, P.Z., K.Z., J.Z. and S.D. All authors have read and agreed to the published version of the manuscript.

Funding: We are grateful for the financial support from Collaborative Innovation Center of Internet+3D Printing in Shanxi Province (CiCi3DP). We thank Scientific Research Foundation of Taiyuan University of Science and Technology (No.20182056, 20192009), Natural Science Foundation for Young Scientists of Shanxi Province (No.

201901D211308), Scientific and Technological Innovation Programs of Higher Education Institutions in Shanxi (No.2019L0652).

Conflicts of Interest: The authors declare no conflict of interest.

References

1. Hasegawa, M.; Horie, K. Photophysics, photochemistry, and optical properties of polyimides. *Prog. Polym. Sci.* **2001**, *26*, 259–335. [[CrossRef](#)]
2. Sazanov, Y.N. Applied significance of polyimides. *Russ. J. Appl. Chem.* **2001**, *74*, 1253–1269. [[CrossRef](#)]
3. Mazoniene, E.; Bendoraitiene, J.; Peculyte, L.; Diliunas, S.; Zemaitaitis, A. (Co) polyimides from commonly used monomers, and their nanocomposites. *Prog. Solid State Chem.* **2006**, *34*, 201–211. [[CrossRef](#)]
4. Ge, J.J.; Zhang, D.; Li, Q.; Hou, H.; Graham, M.J.; Dai, L.; Cheng, S.Z. Multiwalled carbon nanotubes with chemically grafted polyetherimides. *J. Am. Chem. Soc.* **2005**, *127*, 9984–9985. [[CrossRef](#)] [[PubMed](#)]
5. Meador, M.A. Recent advances in the development of processable high-temperature polymers. *Annu. Rev. Mater. Sci.* **1998**, *28*, 599–630. [[CrossRef](#)]
6. Chung, I.S.; Park, C.E.; Ree, M.; Kim, S.Y. Soluble polyimides containing benzimidazole rings for interlevel dielectrics. *Chem. Mater.* **2001**, *13*, 2801–2806. [[CrossRef](#)]
7. Tagawa, M.; Maeda, K.I.; Kajita, T.; Yokota, K.; Akamatsu, K.; Nawafune, H. Atomic beam-induced fluorination of polyimide and its application to site-selective Cu metallization. *Langmuir* **2007**, *23*, 11351–11354. [[CrossRef](#)]
8. Liaw, D.J.; Wang, K.L.; Huang, Y.C.; Lee, K.R.; Lai, J.Y.; Ha, C.S. Advanced polyimide materials: Syntheses, physical properties and applications. *Prog. Polym. Sci.* **2012**, *37*, 907–974. [[CrossRef](#)]
9. Guo, Y.; Lyu, Z.; Yang, X.; Lu, Y.; Ruan, K.; Wu, Y.; Gu, J. Enhanced thermal conductivities and decreased thermal resistances of functionalized boron nitride/polyimide composites. *Compos. Part B Eng.* **2019**, *164*, 732–739. [[CrossRef](#)]
10. Matsuura, T.; Hasuda, Y.; Nishi, S.; Yamada, N. Polyimide derived from 2, 2'-bis (trifluoromethyl)-4, 4'-diaminobiphenyl. 1. Synthesis and characterization of polyimides prepared with 2, 2'-bis (3, 4-dicarboxyphenyl) hexafluoropropane dianhydride or pyromellitic dianhydride. *Macromolecules* **1991**, *24*, 5001–5005. [[CrossRef](#)]
11. Jiang, X.; Bin, Y.; Matsuo, M. Electrical and mechanical properties of polyimide-carbon nanotubes composites fabricated by in situ polymerization. *Polymer* **2005**, *46*, 7418–7424. [[CrossRef](#)]
12. Bin, Y.; Oishi, K.; Koganemaru, A.; Zhu, D.; Matsuo, M. Catalytic effect of nickel under carbonization of polyimide films. *Carbon* **2005**, *43*, 1617–1627. [[CrossRef](#)]
13. Guo, Y.; Yang, X.; Ruan, K.; Kong, J.; Dong, M.; Zhang, J.; Guo, Z. Reduced graphene oxide heterostructured silver nanoparticles significantly enhanced thermal conductivities in hot-pressed electrospun polyimide nanocomposites. *ACS Appl. Mater. Interfaces* **2019**, *11*, 25465–25473. [[CrossRef](#)] [[PubMed](#)]
14. Hsiao, S.H.; Chen, Y.J. Structure–property study of polyimides derived from PMDA and BPDA dianhydrides with structurally different diamines. *Eur. Polym. J.* **2002**, *38*, 815–828. [[CrossRef](#)]
15. Feger, C.; Khojasteh, M.M.; Htoo, M.S. *Advances in Polyimide Science and Technology*; Technomic Press: Lancaster, UK, 1993; pp. 15–32. ISBN 0-87762-983-8.
16. Ghosh, M. *Polyimides: Fundamentals and Applications*; Marcel Dekker Press: New York, NY, USA, 1996; p. 471. ISBN 0-8247-9466-4.
17. Mittal, K.L. *Polyimides: Synthesis, Characterization and Applications*; Springer Science & Business Media Press: New York, NY, USA, 1982; p. 537. ISBN 978-1-4615-7639-6.
18. Stenzenberger, H.D.; Hergenrother, P.M. *Polyimides*; Springer Science & Business Media Press: New York, NY, USA, 1990; p. 34. ISBN 978-94-010-9663-8.
19. Hasegawa, M.; Sensui, N.; Shindo, Y.; Yokota, R. Structure and properties of novel asymmetric biphenyl type polyimides. Homo- and copolymers and blends. *Macromolecules* **1999**, *32*, 387–396. [[CrossRef](#)]
20. Smith, Z.P.; Hernández, G.; Gleason, K.L.; Anand, A.; Doherty, C.M.; Konstas, K.; Freeman, B.D. Effect of polymer structure on gas transport properties of selected aromatic polyimides, polyamides and TR polymers. *J. Membr. Sci.* **2015**, *493*, 766–781. [[CrossRef](#)]
21. Chang, J.; Niu, H.; Zhang, M.; Ge, Q.; Li, Y.; Wu, D. Structures and properties of polyimide fibers containing ether units. *J. Mater. Sci.* **2015**, *50*, 4104–4114. [[CrossRef](#)]

22. Coletta, E.; Toney, M.F.; Frank, C.W. Effects of aromatic regularity on the structure and conductivity of polyimide-poly (ethylene glycol) materials doped with ionic liquid. *J. Polym. Sci. Part B Polym. Phys.* **2015**, *53*, 509–521. [[CrossRef](#)]
23. Tamai, S.; Yamaguchi, A.; Ohta, M. Melt processible polyimides and their chemical structures. *Polymer* **1996**, *37*, 3683–3692. [[CrossRef](#)]
24. Chen, G.; Wang, X.; Lin, J.; Yang, W.; Li, H.; Wen, Y. Interfacial polarity modulation of $\text{KTa}_{0.5}\text{Nb}_{0.5}\text{O}_3$ nanoparticles and its effect on dielectric loss and breakdown strength of poly (vinylidene fluoride) nanocomposites with high permittivity. *J. Phys. Chem. C* **2016**, *120*, 28423. [[CrossRef](#)]
25. Chen, G.; Wang, X.; Lin, J.; Yang, W.; Li, H.; Wen, Y.; Lei, Q. Nano-KTN@ Ag/PVDF composite films with high permittivity and low dielectric loss by introduction of designed KTN/Ag core/shell nanoparticles. *J. Mater. Chem. C* **2016**, *4*, 8070–8076. [[CrossRef](#)]



© 2020 by the authors. Licensee MDPI, Basel, Switzerland. This article is an open access article distributed under the terms and conditions of the Creative Commons Attribution (CC BY) license (<http://creativecommons.org/licenses/by/4.0/>).